JP2.5 A technique for creating composite sea surface temperatures from NASA's MODIS instruments in order to improve numerical weather prediction

Jason C. Knievel,* Daran L. Rife, Joseph A. Grim,
Andrea N. Hahmann,† Joshua P. Hacker, Ming Ge, and Henry H. Fisher
National Center for Atmospheric Research, Boulder, Colorado, USA

1. Introduction

Numerical simulations of the atmosphere above and near large bodies of water are sensitive to how the water's skin temperature is specified (e.g., Thiébaux et al. 2003; Pullen et al. 2007; LaCasse et al. 2008; Song et al. 2009). The goal of this paper is to describe a simple method of creating composites of lake- and sea-surface temperature (LST and SST) based on datasets distributed by the National Aeronautics and Space Administration (NASA) and derived from the Moderate Resolution Imaging Spectroradiometer (MODIS) aboard each of the polar orbiting *Aqua* and *Terra* satellites. The composite is constructed from data typically available nearly in real time; applicable anywhere on the globe, including over inland bodies of water; has a spatial resolution similar to that of the typical operational, nested NWP model; is accurate near coasts; and is capable of representing, at least roughly, the diurnal cycle in skin temperature. This last feature is not yet fully implemented at the time of writing but will be generally described in the paper's last section.

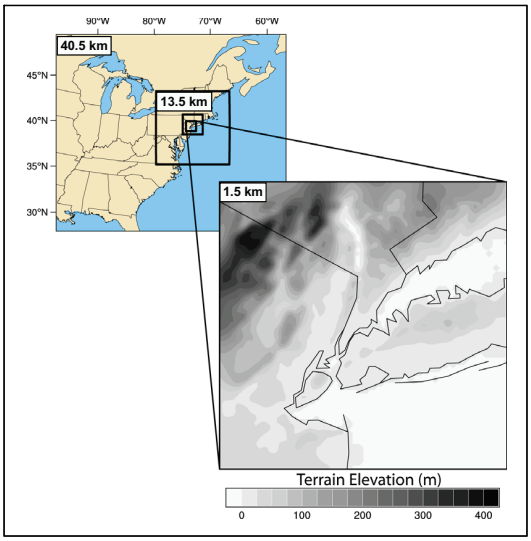

Figure 1: The four computational domains used for the numerical simulations. The domains' respective grid intervals are 40.5, 13.5, 4.5, and 1.5 km. For the sake of clarity, the interval of domain 3 is not labeled on the figure.

2. Data

2.1 MODIS data

Swaths observed by the MODIS aboard *Aqua* and *Terra* cover a given location on the globe roughly twice per day. From the observed radiances, NASA produces a variety of SST products (Esaias et al. 1998). For this work we use two of the Level 3 products: daily daytime SSTs and daily nighttime SSTs. NASA's Level 3 products are geo-referenced, two-dimensional arrays of satellite data on a global, equal-area grid with cells of 4.6×4.6 kilometers. For our purposes, the Level 3 data offered several advantages over Level 2 data—more extensive quality control and geo-referencing, in particular.

A file of NASA's Level 3 daytime SST comprises the arithmetic mean of skin temperatures observed in a 24-hr period along the parts of satellite overpasses made during local daytime. The daily nighttime files comprise the corresponding temperatures observed during nighttime. NASA computes skin temperature with two algorithms, one based on short-wave brightness temperatures at 3.959 and 4.050μm, and another based on long-wave brightness temperatures at 11.0172 and 12.0324μm (Franz 2006). The short-wave algorithm is used only for nighttime SST because sun glint during the day corrupts the retrievals. The long-wave algorithm is valid during both day and night, so it is the long-wave SST products that we used for this work.

2.2 Real-time global (RTG) SST data

The second SST dataset that we employ is the Real-Time Global (RTG) Analysis from the Marine Modeling and Analysis Branch (MMAB) of the National Centers for Environmental Prediction (NCEP). The daily analyses are created from a two-dimensional variational analysis of data from buoys, ships, and satellites over the preceding 24 hours (Thiébaux et al. 2003; Gemmill et al. 2007). The product is incorporated into operational models such as the North American Model (NAM) and the global forecast model at the European Center for Medium Range Weather Forecasting (ECMWF). Since January 2001 the RTG Analysis has been available daily on a grid with pixel size of 1/2° latitude and longitude. In September 2005 a 1/12° product became available. Cur-

*Corresponding author: Dr. Jason Knievel, NCAR, 3450 Mitchell Lane, Boulder, CO, USA 80301; knievel@ucar.edu.

†Dr. Hahmann is now at Risø National Laboratory for Sustainable Energy, Technical University of Denmark.

rently, NCAR downloads every day the analyses at both resolutions, using the finer unless it is unavailable.

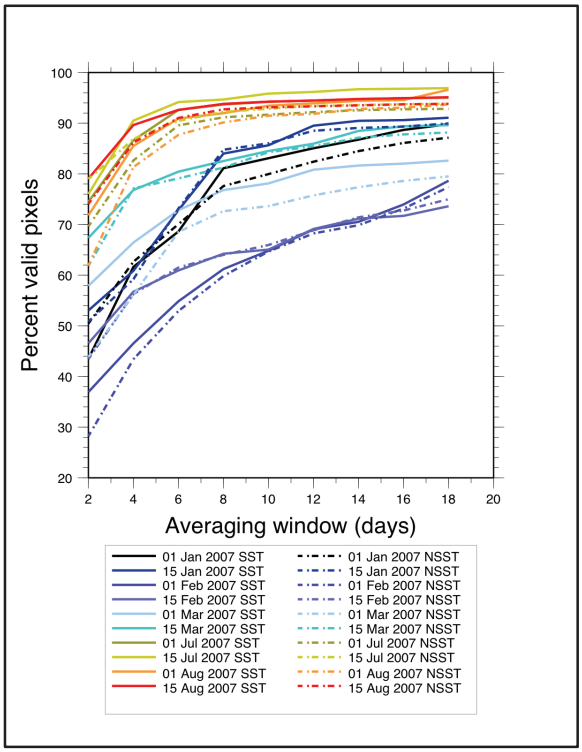

Figure 2: Percentage of cells on the MODIS Level 3 grid within the outermost computational domain (Fig. 1) that are filled (i.e., not missing) as a function of the number of days of data that compose the temporal composite. Each colored line applies to periods of time ending on the dates listed in the key. Values for daytime retrievals are solid and for nighttime are dashed.

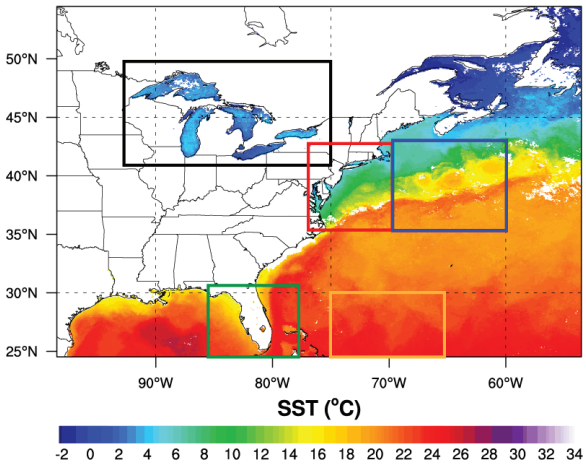

Figure 3: Regions used for calculation of the autocorrelations of SST in Fig. 4.

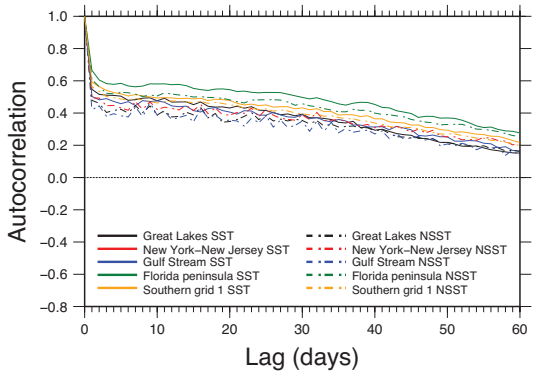

Figure 4: Autocorrelation of SST on the MODIS Level 3 grid as a function of number of days of data that compose the temporal composite. Values for daytime retrievals are solid and for nighttime are dashed.

3. Numerical model

To design and test our method of creating SST composites we used the Advanced Research core of the Weather Research and Forecasting (WRF) Model version 3.0.1.1 (Skamarock et al. 2005) and the Real-Time Four-Dimensional Data Assimilation (RTFDDA) system (Liu et al. 2008).

The four one-way nested computational domains are shown in Fig. 1. Physical parameterizations include the Yonsei University (YSU) planetary boundary layer (PBL) scheme, the Noah land-surface model, the Monin-Obhukov surface-layer scheme, the new Kain-Fritsch cumulus scheme, the Lin microphysics scheme, Dudhia short-wave radiation, and Rapid Radiative Transfer Model (RRTM) long-wave radiation. Explicit sixth-order diffusion is weakly applied, with the monotonic constraint. Initial and lateral boundary conditions are from the Global Forecast System (GFS) operated by NCEP.

4. SST composite

Creation of our composite SST fields involves five steps, each designed to overcome, or at least mitigate, inherent inadequacies in the individual daily Level 3 files from a single satellite. During these steps, daytime and nighttime data are treated identically and processed in parallel to produce two composite SST fields for each date. Which of the two composite fields is introduced into the WRF Model during assimilation will depend on whether it is day or night on the finest computational domain when the lower boundary conditions are updated during a simulation. At the time of writing, the nighttime SSTs are not fully implemented.

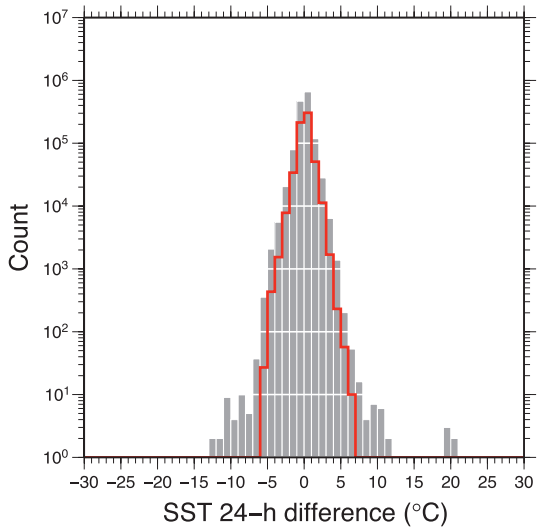

Figure 5: Histogram of 24-h changes in daytime SST on the MODIS grid over the subregion of interest. This example is for the period ending 26 April 2006. The isolated values near 20°C, and the two lobes centered near ±10°C in the tails of the main distribution are treated as erroneous retrievals in the original Level 3 data. The red contour outlines the histogram calculated after an additional layer of quality control is applied, which removes SSTs that differ by ≥6°C from the values on both neighboring days.

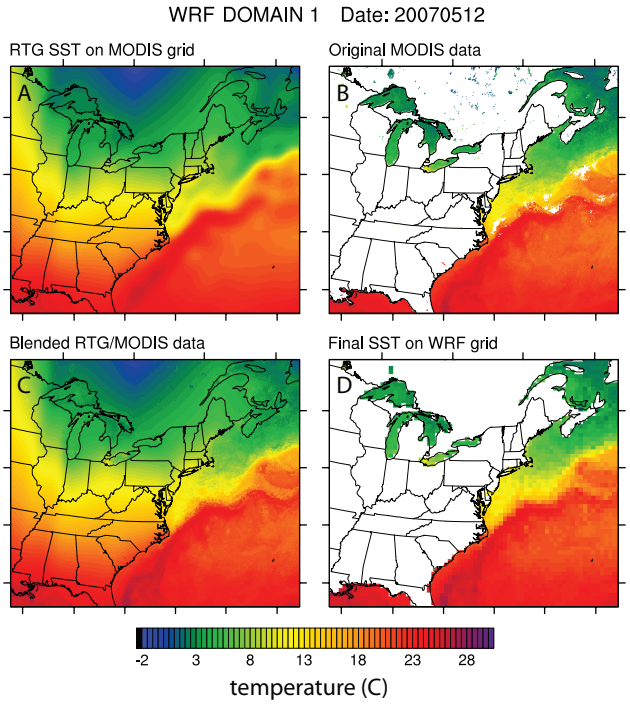

Figure 6: Graphical depiction of how the RTG and MODIS data are blended to define the WRF Model's lower boundary condition. The RTG dataset includes skin temperature over land but the MODIS dataset does not. This example is from 12 May 2007. The panels depict: a) RTG data used as the background field, b) 12-day composite of data from *Aqua* and *Terra*, c) combined field in which holes in the MODIS data are filled with RTG data, and d) the combined field mapped to the coarsest of the WRF Model's four computational grids, with data over land excluded.

In the first step, each day's Level 3 data from *Aqua* and *Terra* are merged into a two-satellite, daily array of skin temperature. It is at this stage that the location and size of the array are restricted to what is necessary for the NWP computational domain. For this paper, the domains are focused on the Mid-Atlantic Seaboard.

Second, the daily files from the prior N days are combined into a multi-day composite. This step is necessary because daily files of IR-based retrievals suffer from large areas in which clouds cause missing data (e.g., Li et al. 2005), even when the files include retrievals from both *Aqua* and *Terra*. For the part of the Atlantic Ocean of interest to us, $N = 12$ days is long enough to capture valid satellite retrievals (Fig. 2), yet short enough to retain most of the physical structure in the ocean's skin temperature, as represented by the autocorrelation of temperature on the MODIS grid (Figs. 3 and 4).

In the third step, we apply one additional layer of quality control beyond the layers that are part of NASA's Level 3 processing. Detection of clouds in IR data is imperfect (e.g., Cayula and Cornillon 1996; Stowe et al. 1999; Chelton and Wentz 2005) so even the heavily processed Level 3 data are occasionally corrupted by cirri, low stratocumuli, and the like. This produces 24-h changes in SST that sometimes are unphysically large (Fig. 5). Observations and simulations with simple models strongly suggest that 24-h changes in skin temperature greater than 6°C over large regions of open ocean are not physical (e.g., Stramma et al. 1986; Webster et al. 1996; Kawai and Kawamura 2002; Minnet 2003). The same is suggested by the lobes in the tails of the main distribution in Fig. 5, to say nothing of the extreme outliers near 20°C. Therefore, while the N=12 days of daily merged data are being combined, any SSTs responsible for a 24-h change greater than 6 °C are set to missing and do not contribute to the 12-day composite. This threshold is somewhat arbitrary—one could probably justify a choice of 4°C or, perhaps less easily, 8°C—but 6°C appears to work well for our purposes.

This additional quality control removes some pixels, and there are inevitably still some holes in SST owing to persistent cloudiness (Figs. 2 and 6b). Accordingly, in the fourth step, holes in the MODIS-based composite are filled with the 12-day mean of NCEP's RTG SST, after removal of any bias between the RTG and MODIS data (Fig. 6). Removing this bias prevents the background field from introducing unphysical extrema when it is used to fill in the MODIS data's holes.

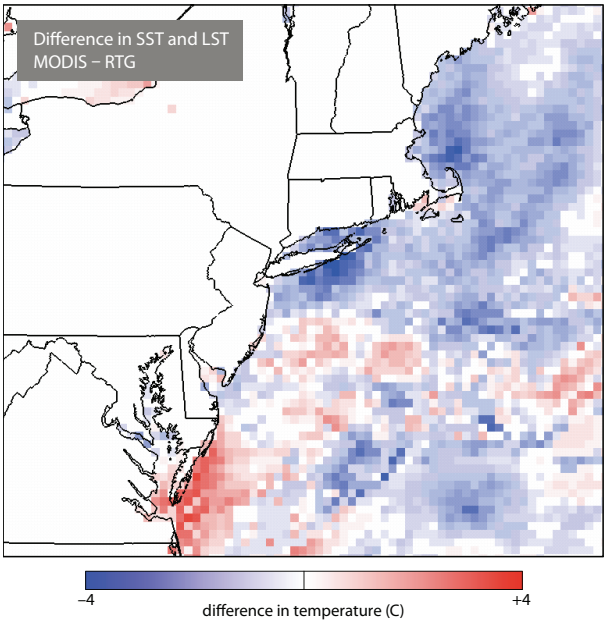

Figure 7: Difference in LST and SST (°C) between the 12-day MODIS composite and the RTG daily file for 12 May 2007 on computational domain 2 of 4.

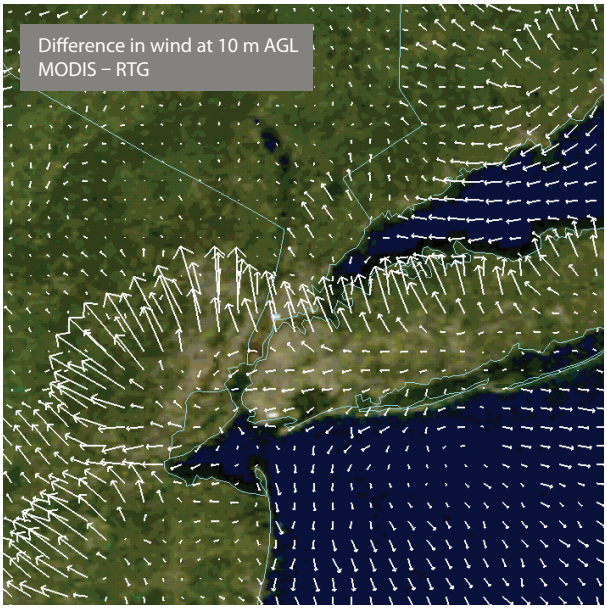

Figure 8: Difference in wind at 10 m AGL between simulations based on the 12-day MODIS composite and the RTG daily file at 1800 UTC on 12 May 2007. The longest vectors represent a difference of approximately 4 m s^{-1}. The figure is a close-up of part of computational domain 3 of 4.

In the fifth and final step, we compensate for the fact that using $N=12$ days of daily merged files (that is, today's merged file plus the files from the last 11 days) to create the composite SST field means that it will lag the seasonal fluctuations in SST by nominally 5.5 days (half of the past 11 days). Even such a relatively short lag can equate to nearly 1°C during times of the year when SSTs change most rapidly. To compensate for this lag, we a) calculate the spatial and temporal mean SST from the 12-day composite of RTG data; b) subtract that value from today's spatial mean of RTG data; then c) add that difference, which is the negative of the mean lag, to every pixel of the 12-day composite MODIS SST field. The lag is best calculated from the RTG data, not the MODIS data itself, because the former has no missing pixels. Missing pixels in the latter can distort the calculation—for example, when most of the missing pixels are over the cold water of the north Atlantic.

Figure 6d shows how the SST field looks once all five steps are completed and the resultant composite is mapped to the model's computation domains.

5. Example simulation

A thorough exploration of how the composite SSTs from MODIS data affect simulations of coastal circulations is beyond the scope of this short paper, as are rigorous analyses of how well the MODIS-based composite verifies against in-situ data and other composites. Even so, it is useful briefly to present a few figures from one case that we are now studying.

Figure 7 shows from 12 May 2007 the difference between SSTs and LSTs from the 12-day MODIS-based composite and those available in the daily RTG files that are used as the background field. (At the time of writing, the 1/12° RTG were not available to us from 2007, so this comparison is based on the 1/2° data.) Differences between the two datasets in this example are 0–4°C. The MODIS-based SSTs are distinctly lower off the coast of Long Island and northward. Off the Delmarva Peninsula, it is the RTG dataset that has lower SSTs.

Not surprisingly, several test simulations of boundary layer wind have proven sensitive to this difference in SST. For example, by 1800 UTC on 12 May (Fig. 8), the sea breeze in the simulation with the MODIS-based composite is farther inland by 10–30 km in many parts of northern New Jersey and Long Island when compared with a simulation with RTG data. Differences in the strength and timing of sea breezes have important implications for air quality and transport and dispersion in coastal urban areas.

6. Future work

We are just now beginning to account for the diurnal cycle in SST by creating separate composites based on

daytime and nighttime Level 3 data. The simplest approach, which we will try first, is to select between the two composites depending on the local solar time at the center of the model's innermost computational domain. We will also test whether it is advantageous to interpolate between the two single states (daytime and nighttime) to approximately represent intermediate SST conditions during the diurnal cycle.

As mentioned in the previous section, verification of the MODIS-based composites against in-situ data, and more detailed exploration of how numerical simulations of weather phenomena are sensitive to the MODIS-based composite SSTs and LSTs, will be the subjects of other work and other papers.

Acknowledgments. This work is being funded by NASA through grant NNS06AA58G, and by the U. S. Army Test and Evaluation Command through an interagency agreement with the National Science Foundation. NCAR is sponsored by the National Science Foundation.

REFERENCES

Cayula, J.-F., and P. Cornillon, 1996: Cloud detection from a sequence of SST images. *Remote Sens. Environ.*, **55**, 80–88.

Chelton, D. B., and F. J. Wentz, 2005: Global microwave satellite observations of sea surface temperature for numerical weather prediction and climate research. *Bull. Amer. Meteor. Soc.*, **86**, 1097–1115.

Esaias, W. E., M. A. Abbott, I. Barton, O. B. Brown, J. W. Campbell, K. L. Carder, D. K. Clark, R. H. Evans, F. E. Hoge, H. R. Gordon, W. M. Balch, R. Letelier, and P. J. Minnett, 1998: An overview of MODIS capabilities for ocean science observations. *IEEE T. Geosci. Remote.*, **36**, 1250–1265.

Franz, B., 2006: Implementation of SST processing within the OBPG. On-line document. [Available at http://oceancolor.gsfc.nasa.gov/DOCS/modis_sst/.]

Gemmill, W., B. Katz, and X. Li, 2007: Daily real-time global sea surface temperature–high resolution analysis at NOAA/NCEP. NOAA/NWS/NCEP/MMAB Office Note No. 260, NOAA/NCEP, 39 pp. [Available at http://polar.ncep.noaa.gov/sst/.]

Kawai, Y., and H. Kawamura, 2002: Evaluation of the diurnal warming of sea surface temperature using satellite-derived marine meteorological data. *J. Oceanogr.*, **58**, 805–814.

LaCasse, K. M., M. E. Splitt, S. M. Lazarus, and W. M. Lapenta, 2008: The impact of high resolution sea surface temperatures on the simulated nocturnal Florida marine boundary layer. *Mon. Wea. Rev.*, **136**, 1349–1372.

Li, J., X. Gao, R. A. Maddox, and S. Sorooshian, 2005: Sensitivity of North American Monsoon rainfall to multisource sea surface temperatures in MM5. *Mon. Wea. Rev.*, **133**, 2922–2939.

Liu, Y., W. T. T, J. F. Bowers, L. P. Carson, F. Chen, C. Clough, C. A. Davis, C. H. Egeland, S. H. Halvorson, T. W. Huck, Jr., L. Lachapelle, R. E. Malone, D. L. Rife, R.-S. Sheu, S. P. Swerdlin, and D. S. Weingarten, 2008: The operational mesogamma-scale analysis and forecast system of the U. S. Army Test and Evaluation Command. Part I: Overview of the modeling system, the forecast products, and how the products are used. *J. Appl. Meteor. Climatol.*, **47**, 1077–1092.

Minnet, P. J., 2003: Radiometric measurements of the sea-surface skin temperature: the competing roles of the diurnal thermocline and the cool skin. *Int. J. Remote Sens.*, **24**, 5033–5047.

Pullen, J., T. Holt, A. F. Blumberg, and R. D. Bornstein, 2007: Atmospheric response to local upwelling in the vicinity of New York-New Jersey Harbor. *J. Appl. Meteor. Climatol.*, **46**, 1031–1052.

Skamarock, W. C., J. B. Klemp, J. Dudhia, D. O. Gill, D. M. Barker, M. G. Duda, X.-Y. Huang, W. Wang, and J. G. Powers, 2005: A description of the Advanced Research WRF version 3. NCAR/TN-475+STR. [Available at http://www.mmm.ucar.edu/wrf/users/docs/arw_v3.pdf.]

Song, Q., D. B. Chelton, S. K. Esbensen, N. Thum, and L. W. O'Neill, 2009: Coupling between sea surface temperature and low-level winds in mesoscale numerical models. *J. Climate*, **22**, 146–164.

Stowe, L. L., P. A. Davis, and E. P. McClain, 1999: Scientific basis and initial evaluation of the CLAVR-1 global clear/cloud classification algorithm for the Advanced Very High Resolution Radiometer. *J. Atmos. Oceanic Technol.*, **16**, 656–681.

Stramma, L., P. Cornillon, R. A. Weller, J. F. Price, and M. G. Briscoe, 1986: Large diurnal sea surface temperature variability: Satellite and in situ measurements. *J. Phys. Oceanogr.*, **16**, 827–837.

Thiébaux, J., E. Rogers, W. Wang, and B. Katz, 2003: A new high-resolution blended global sea surface temperature analysis. *Bull. Amer. Meteor. Soc.*, **84**, 645–656.

Webster, P. J., C. A. Clayson, and J. A. Curry, 1996: Clouds, radiation, and the diurnal cycle of sea surface temperature in the tropical weather Pacific. *J. Climate*, **9**, 1712–1730.